

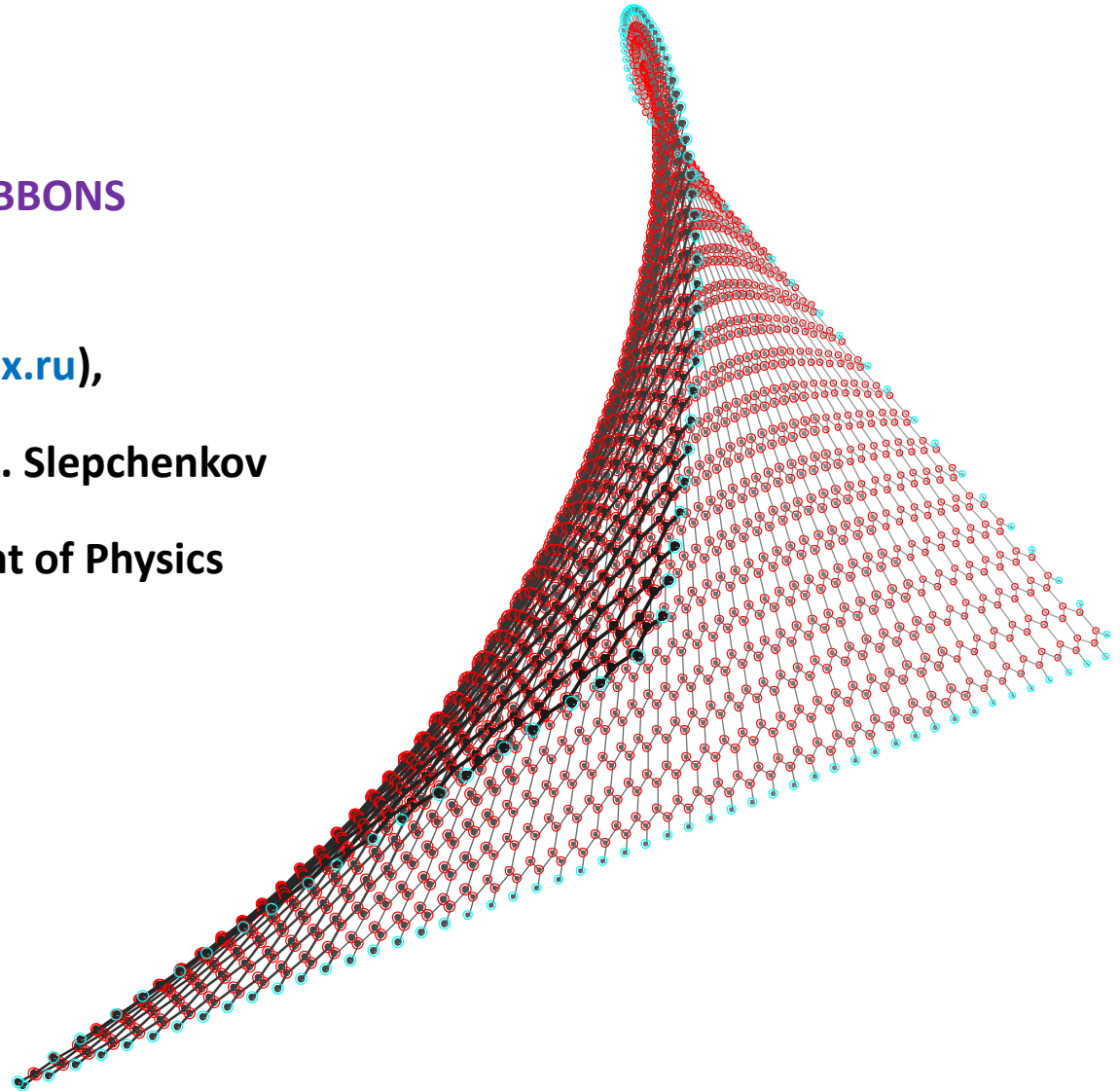
**ELASTIC PROPERTIES
OF GRAPHENE-GRAPHANE NANORIBBONS**

Olga E. Glukhova (graphene@yandex.ru),

I.N. Saliy, A.S. Kolesnikova and M.M. Slepchenkov

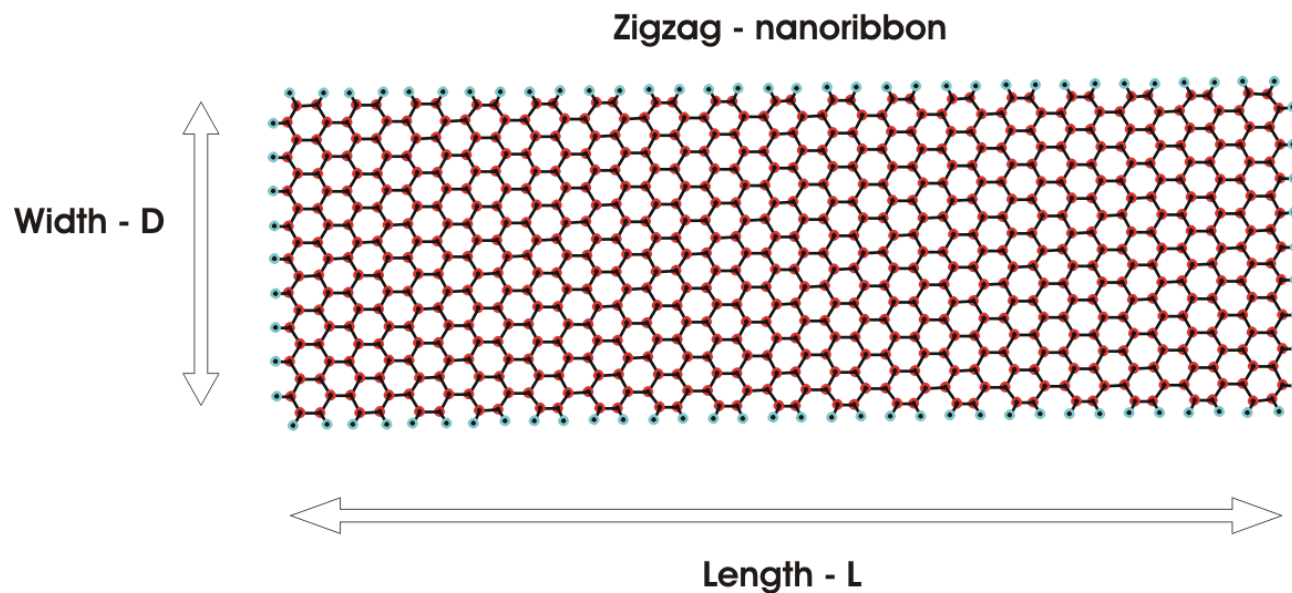
Saratov State University, Department of Physics

410012, Saratov, Russia



Graphene-nanoribbons

We have studied some graphene-nanoribbons with length-to-width ratio L/D from 2 to 3.22. So, nanostructures with ratio L/D less than 3 are classified as nanoparticles, nanoribbons with ratio more than 3 are classified as nanoribbons.



Deformations and elastic properties: empirical study

Computational method

The entire system energy is described by the sum of the binding energy E_b , the torsional energy E_{tors} and the van der Waals energy E_{vdW} :

$$E_{tot} = E_b + E_{tors} + E_{vdW}. \quad (1)$$

In order to study the elastic properties and deformations of graphene-graphane nanoribbons we applied the empirical method based on the bond-order potential developed by Brenner ().

To describe the interaction between the atom and its environment we introduce three different regions in topological network (see Figure 1). As shown in Fig.1, there are near (first), far (third) and intermediate (second) regions about atom with number i .

Atoms from near region are covalently bonded with atom i , atoms from other regions are non-bonded with atom i . The far region has no borders.

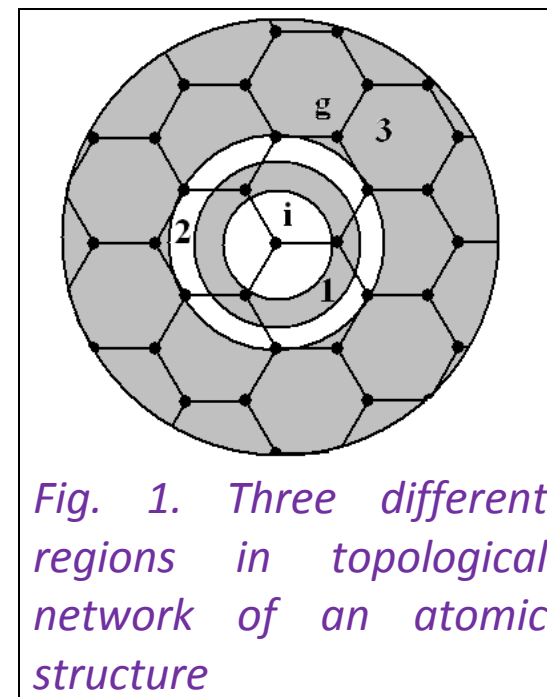


Fig. 1. Three different regions in topological network of an atomic structure

Each pair of covalently bonded atoms interacts via a potential-energy:

$$E_b = \frac{1}{2} \sum_{i=1}^{\text{Nat}} \left(\sum_{j(\neq i)} (V_R(r_{ij}) - B_{ij} V_A(r_{ij})) \right). \quad (2)$$

This is the binding energy. Here V_R is the repulsive pair term, V_A is the attractive pair term, r_{ij} is the distance between the atom with number i and atom j from near region. The function B_{ij} is the many-body term. This term was introduced to describe the specificity of the σ - π interaction. So, the value of the binding energy depends on the position and chemical identity of atoms.

The torsional potential is given by the formula

$$E^{\text{tors}} = \frac{1}{2} \sum_{i=1}^{\text{Nat}} \left(\sum_{j \neq i} \left(\sum_{k \neq i, j} \left(\sum_{l \neq i, j, k} V_{\text{tors}}(\omega_{ijkl}) \right) \right) \right). \quad (3)$$

The torsional potential $V_{\text{tors}}(\omega_{ijkl})$ is given as a function of a dihedral angle ω . The torsion angle ω_{ijkl} is defined in the usual way as the angle between the plane defined by the vectors \mathbf{r}_{ik} and \mathbf{r}_{ij} and that defined by \mathbf{r}_{ij} and \mathbf{r}_{jl} . Here atoms j and k are given from intermediate (second) region and the atom l is given from far region.

Van der Waals energy E_{vdW} defines the interaction between non-bonded atoms:

$$E_{\text{vdW}} = \frac{1}{2} \sum_{i=1}^{\text{Nat}} \left(\sum_{j(\neq i)} V_{\text{vdW}}(r_{ij}) \right). \quad (4)$$

Van der Waals interaction energy may be described by the Lennard-Jones, Morse, Buckingham potentials and so on. We have implemented and compared Lennard-Jones and Morse potentials as functions to define the van der Waals energy. We use Morse potential that is given by

$$V_{\text{Morse}}(r_{ij}) = D_e \left(\left(1 - \exp(-\beta(r_{ij} - r_e)) \right)^2 - 1 \right) + E_r \cdot \exp(-\beta' r_{ij}), \quad (5)$$

where D_e is the average bond energy, E_r is the repulsion nucleus energy, β, β' - parameters.

Algorithm of the calculation of the Young's pseudo-modulus

- 1) Optimization of atomic structure by entire system energy minimization (Eq.1) on atomic coordinates (the atomic structure obtained from previous optimization);
- 2) tension or compression of the atomic network of nanoribbon and reoptimization of atomic structure with atoms fixed on the nanoribbon ends;
- 3) for the elastic tension of nanoribbon on 1% the Young's pseudo-modulus is calculated on formula:

$$Y_p = \frac{F L}{D \Delta L}, \quad (6)$$

where a deformation force is given by

$$F = \frac{2\Delta E}{\Delta L}. \quad (7)$$

Here ΔE is the strain energy, namely, the total energy at a given axial strain minus the total energy.

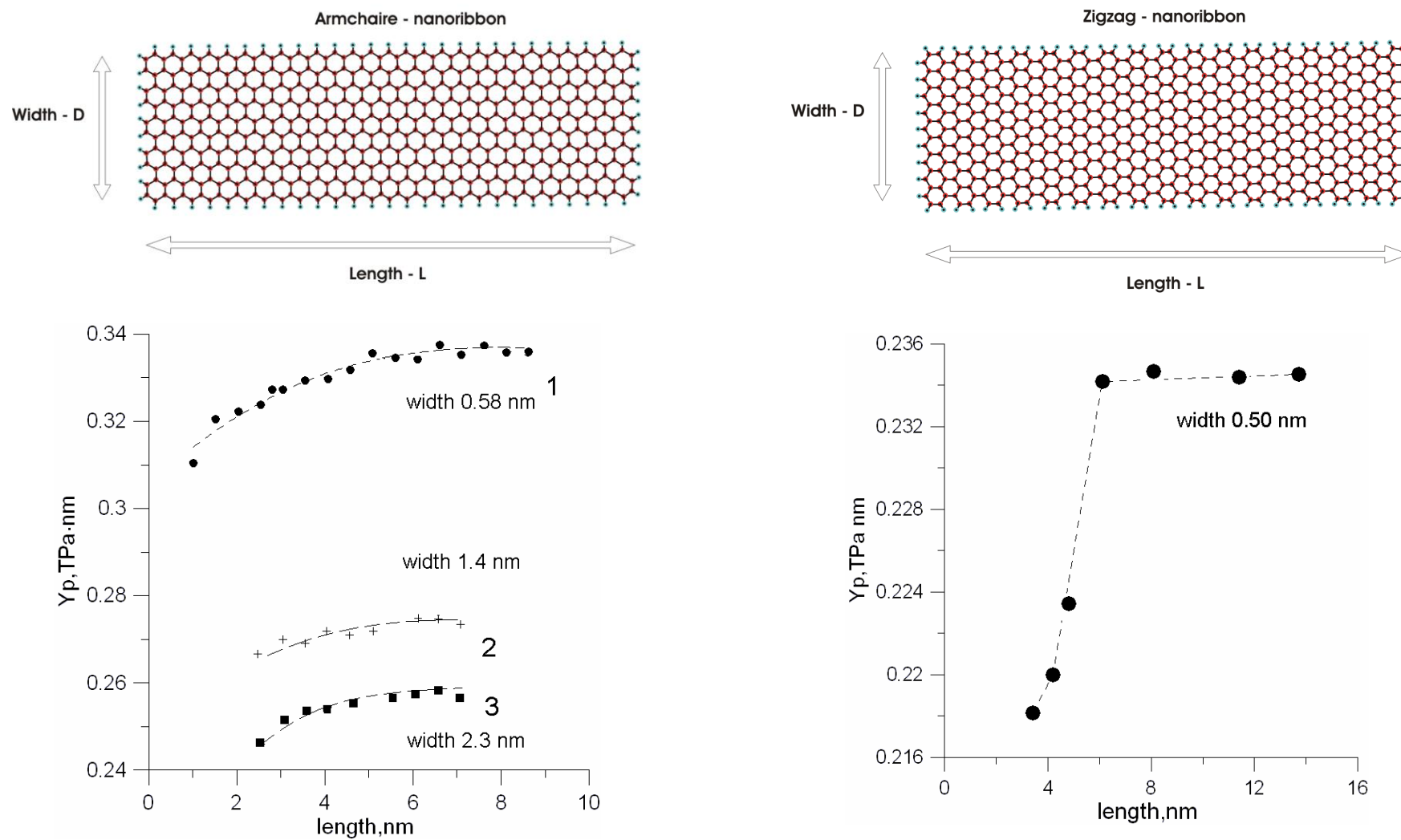
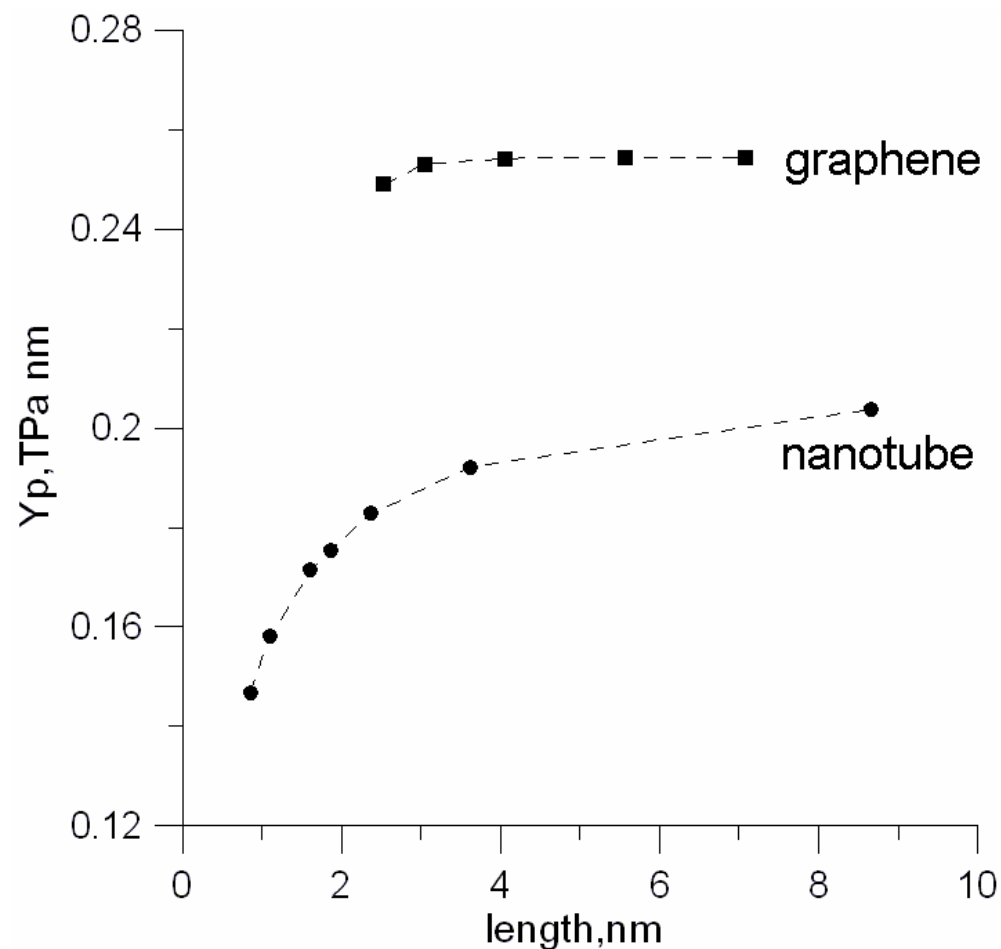


Fig.2. Young's pseudo-modulus of the nanoribbons

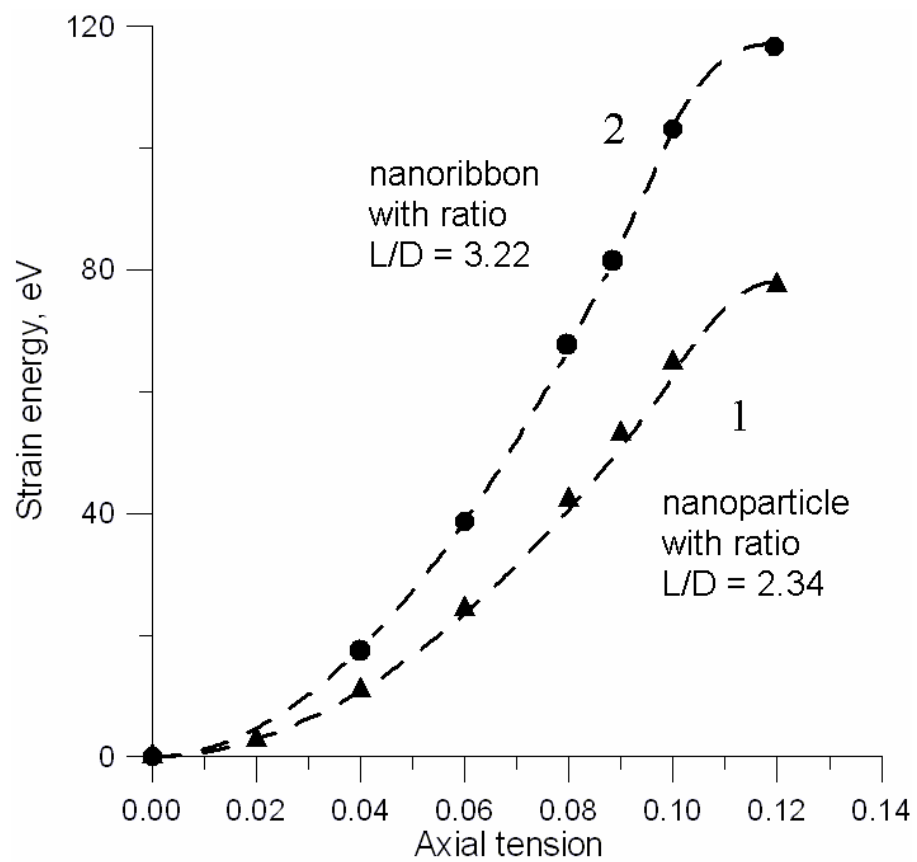


We have compared the elastic properties of the carbon nanotube and the nanoribbon with the same width.

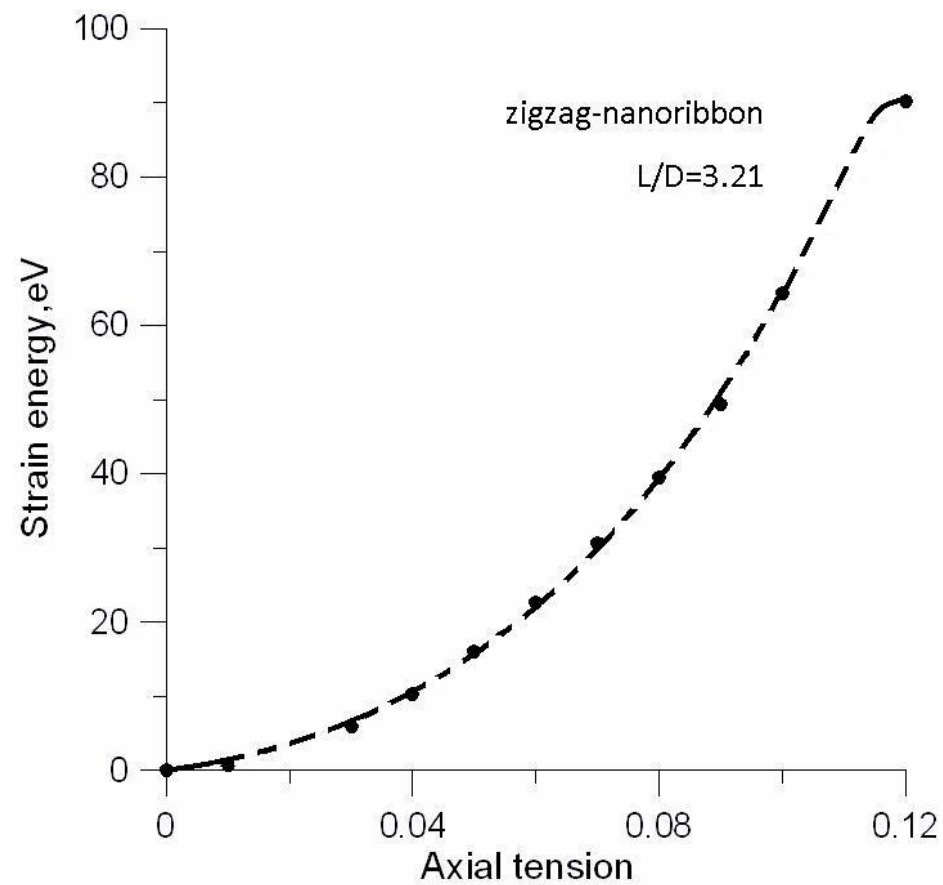
We have calculated the Young's pseudo-modulus of the nanotube (5,5) with the perimeter about 2.1 nm and of the armchair-nanoribbon with the width 2.3 nm.

Young's pseudo-modulus of the armchair-nanoribbon is more than modulus of the nanotube on 27 %.

Fig.3. Strain energy of nanoribbons undergoing axial tension

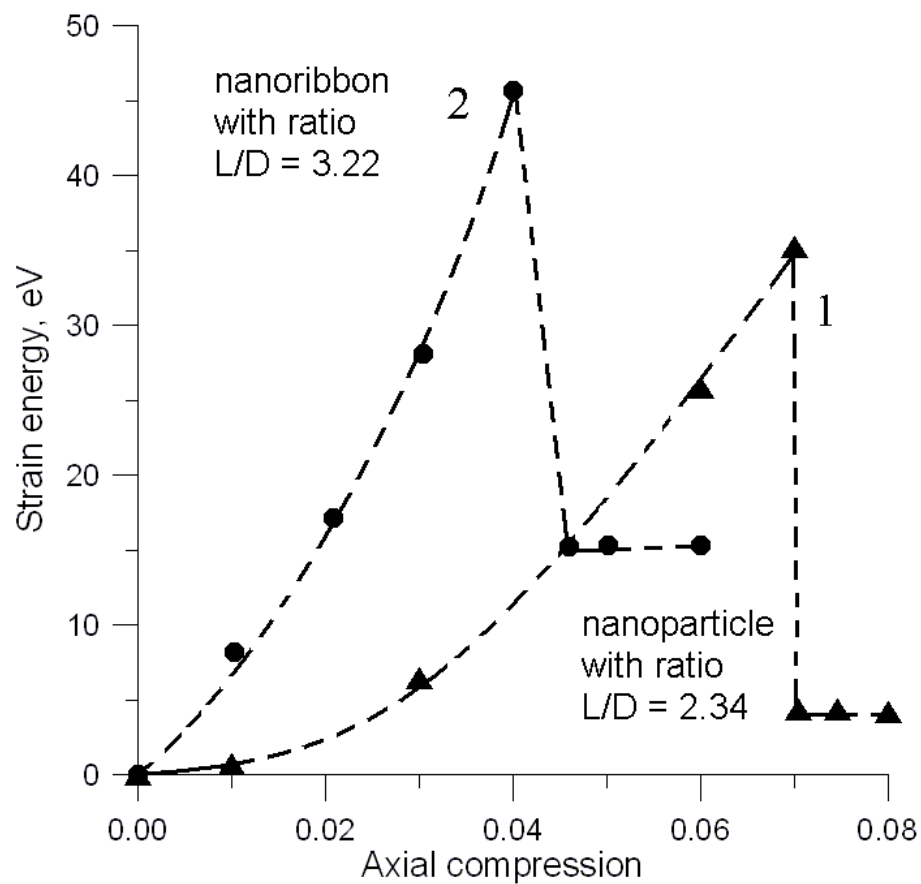


a) Armchair-nanoribbons

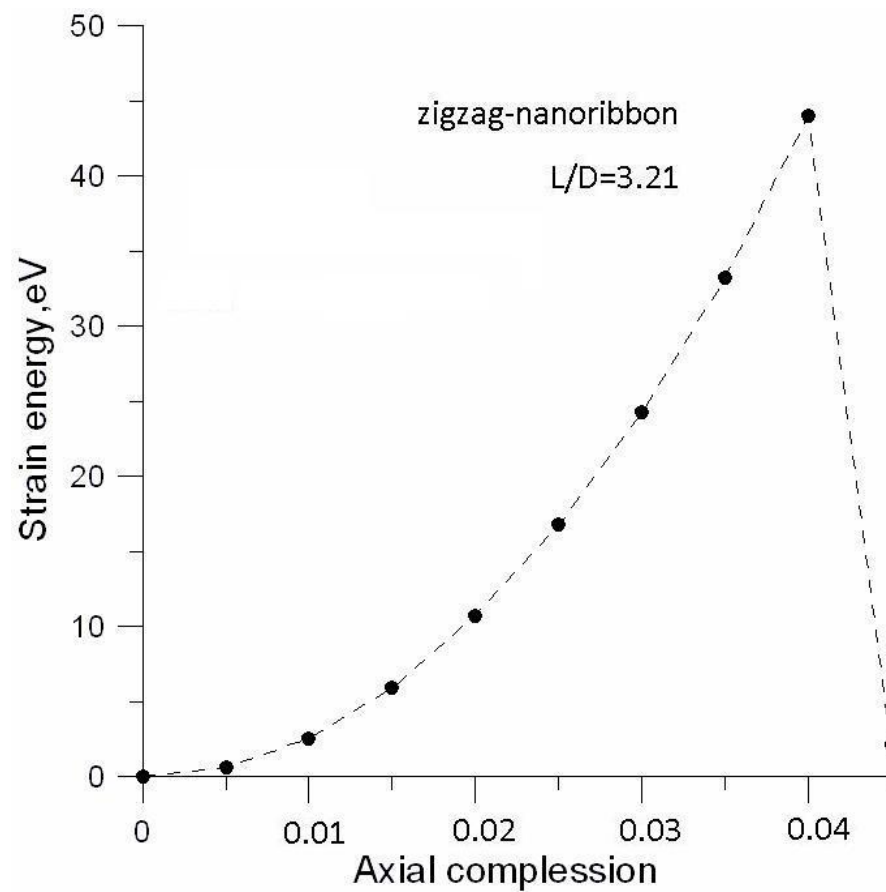


b) zigzag-nanoribbons

Fig.4. Strain energy of nanoribbons undergoing axial tension



a) Armchair-nanoribbons



b) zigzag-nanoribbons

Fig.5. Strain energy of nanoribbons undergoing axial compression

Deformations and elastic properties: quantum study

The TB method was earlier implemented to study a stability of carbon. The energy of a system of ion cores and valence electrons is written as

$$E_{\text{tot}} = E_{\text{bond}} + E_{\text{rep}}. \quad (8)$$

Here the term E_{bond} is the bond structure energy that is calculated as the sum of energies of the single-particle occupied states. Those single-particle energies are known by solving the Schrodinger equation

$$\mathbf{H} |\psi_n\rangle = \varepsilon_n |\psi_n\rangle, \quad (9)$$

where \mathbf{H} is the one-electron Hamiltonian, ε_n is the energy of the n th single-particle state.

The wave functions $|\psi_n\rangle$ can be approximated by linear combination

$$|\psi_n\rangle = \sum_{l\alpha} C_{l\alpha}^n |\phi_{l\alpha}\rangle, \quad (10)$$

where $\{\phi_{l\alpha}\}$ is an orthogonal basis set, l is the quantum number index and α labels the ions. For carbon compounds the matrix elements are calculated as

$$V_{\alpha\beta}(r) = V_{\alpha\beta}^0 \left(\frac{p_3}{r} \right)^{p_1} \exp \left\{ p_1 \left[- \left(\frac{r}{p_2} \right)^{p_4} + \left(\frac{p_3}{p_2} \right)^{p_4} \right] \right\}, \quad (11)$$

where r is the distance between atoms.

Term E_{rep} in Eq.(8) is the phenomenon energy that is a repulsive potential. It can be expressed as a sum of two-body potentials as

$$E_{\text{rep}} = \sum_{\alpha, \beta} V_{\text{rep}}(r_{\alpha\beta}), \quad (12)$$

where V_{rep} is pair potential between atoms at α and β . This two-body potential describes an interaction between bonded and nonbonded atoms and is presented in [8]

$$V_{\text{rep}}(r) = p_5 \left(\frac{p_3}{r} \right)^{p_6} \exp \left\{ p_6 \left[- \left(\frac{r}{p_2} \right)^{p_4} + \left(\frac{p_3}{p_2} \right)^{p_4} \right] \right\} \quad (13)$$

where i and j are orbital moments of wave function, γ presents the bond type (σ or π).

The values of the parameters $V_{\alpha\beta}^0$, the atomic terms and p_n for carbon compounds are given in table.

Table 1

ε_s, eB	ε_p, eB	$V_{ss\sigma}^0, \text{eB}$	$V_{sp\sigma}^0, \text{eB}$	$V_{pp\sigma}^0, \text{eB}$	$V_{pp\pi}^0, \text{eB}$
-10,932	-5,991	-4,344	3,969	5,457	-1,938
p_1	$p_2, \text{\AA}$	$p_3, \text{\AA}$	p_4	p_5, eB	p_6
2,796	2,32	1,54	22	10,92	4,455

Parameters were fitted from experimental data for fullerenes and carbon nanotubes. Transferability to other carbon compounds was tested by comparison with *ab initio* calculations and experiments.

Our transferable tight-binding potential can correctly reproduce changes in the electronic configuration as a function of the local bonding geometry around each carbon atom.

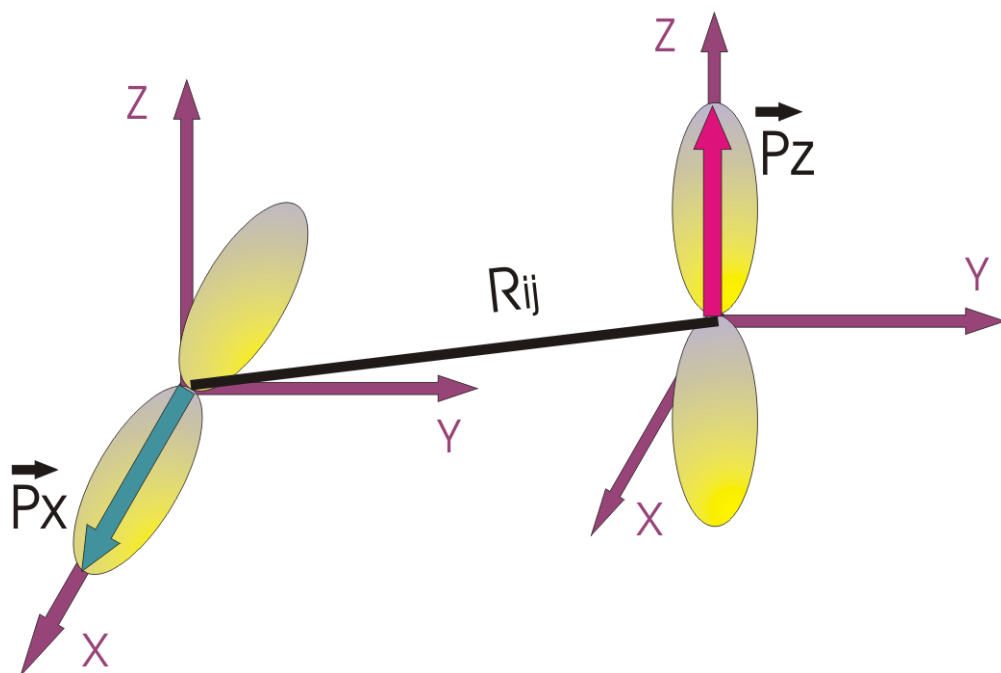


Fig. 6. Schematic representation of the interaction of P_z - and P_x - orbital.

All s- and P-orbitals are given in the real Cartesian coordinates system. To correctly reproduce changes in the electronic configuration of the local bonding geometry around each atom we have defined P-orbital as the axial vector. Each axial vector makes the angle with an direction R_{ij} (α, β, θ) and may be written as the geometrical sum of the two vectors:

$$\begin{aligned}\vec{P}_x &= \vec{P}_{xD} + \vec{P}_{x\perp}, \quad \vec{P}_y = \vec{P}_{yD} + \vec{P}_{y\perp}, \quad (14) \\ \vec{P}_z &= \vec{P}_{zD} + \vec{P}_{z\perp}.\end{aligned}$$

Here \vec{P}_{xD} , \vec{P}_{yD} , \vec{P}_{zD} are projections to an iteratomic direction, $\vec{P}_{x\perp}$... are projections to an orthogonal direction.

So, to describe the interaction between P_z and P_x (see Fig.) we must write:

$$\begin{aligned}\vec{P}_x \cdot \vec{P}_z &= \vec{P}_{xD} \cdot \vec{P}_{zD} \quad + \quad \vec{P}_{x\perp} \cdot \vec{P}_{z\perp} \quad . \quad (15) \\ &\quad \sigma\text{-bonding} \quad \quad \quad \pi\text{-bonding}\end{aligned}$$

Angle between projections \vec{P}_{xD} and \vec{P}_{zD} is equal to zero, but an angle between projections to an orthogonal direction is not zero and it is equal to γ (see Fig.). As a result of some mathematical transformations we can write the expressions for $\cos\gamma$ and the energy of the interaction between P_z and P_x :

$$\cos\gamma = -\frac{\cos\alpha \cdot \cos\theta}{\sin\alpha \cdot \sin\theta}, \quad (16)$$

$$\begin{aligned} V_{P_x P_z}(r_{ij}) &= V_{P_x P_z}^{\sigma}(r_{ij}) \cdot \cos\alpha \cdot \cos\theta + V_{P_x P_z}^{\pi}(r_{ij}) \cdot \sin\alpha \cdot \sin\theta \cdot \cos\gamma = \\ &= V_{P_x P_z}^{\sigma}(r_{ij}) \cdot \cos\alpha \cdot \cos\theta + V_{P_x P_z}^{\pi}(r_{ij}) \cdot \sin\alpha \cdot \sin\theta \cdot \left(-\frac{\cos\alpha \cdot \cos\theta}{\sin\alpha \cdot \sin\theta}\right) = \\ &= \cos\alpha \cdot \cos\theta \left(V_{P_x P_z}^{\sigma}(r_{ij}) - V_{P_x P_z}^{\pi}(r_{ij}) \right) \end{aligned} \quad (17)$$

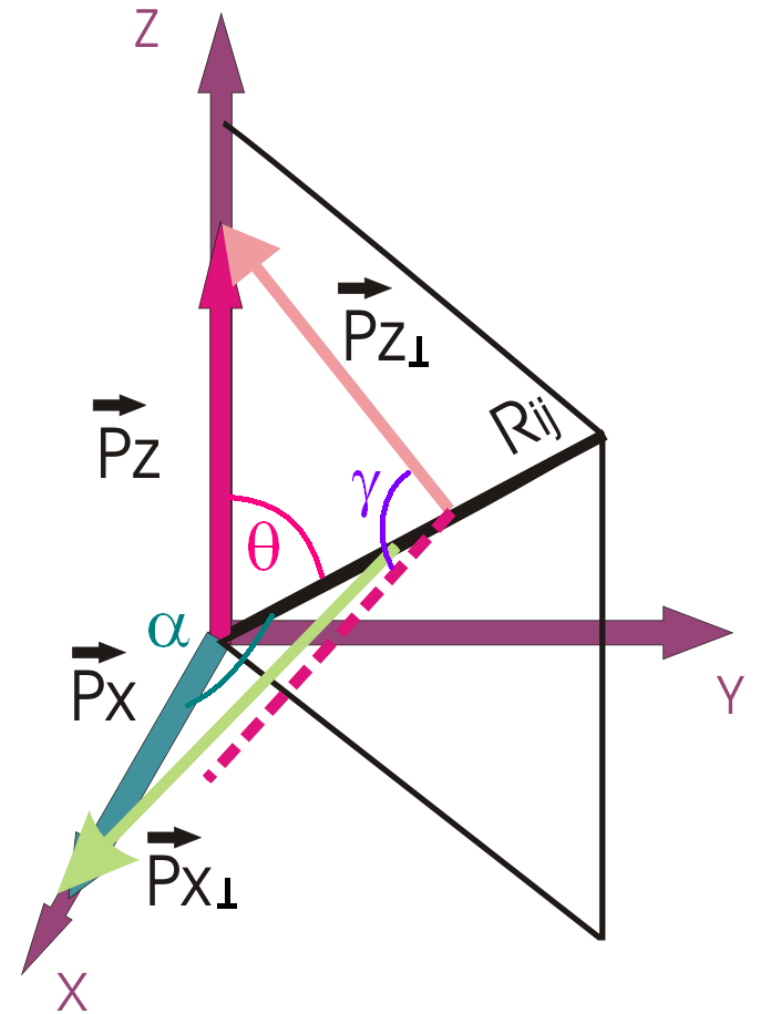


Fig. 7. Projections of P_z - and P_x - vectors.

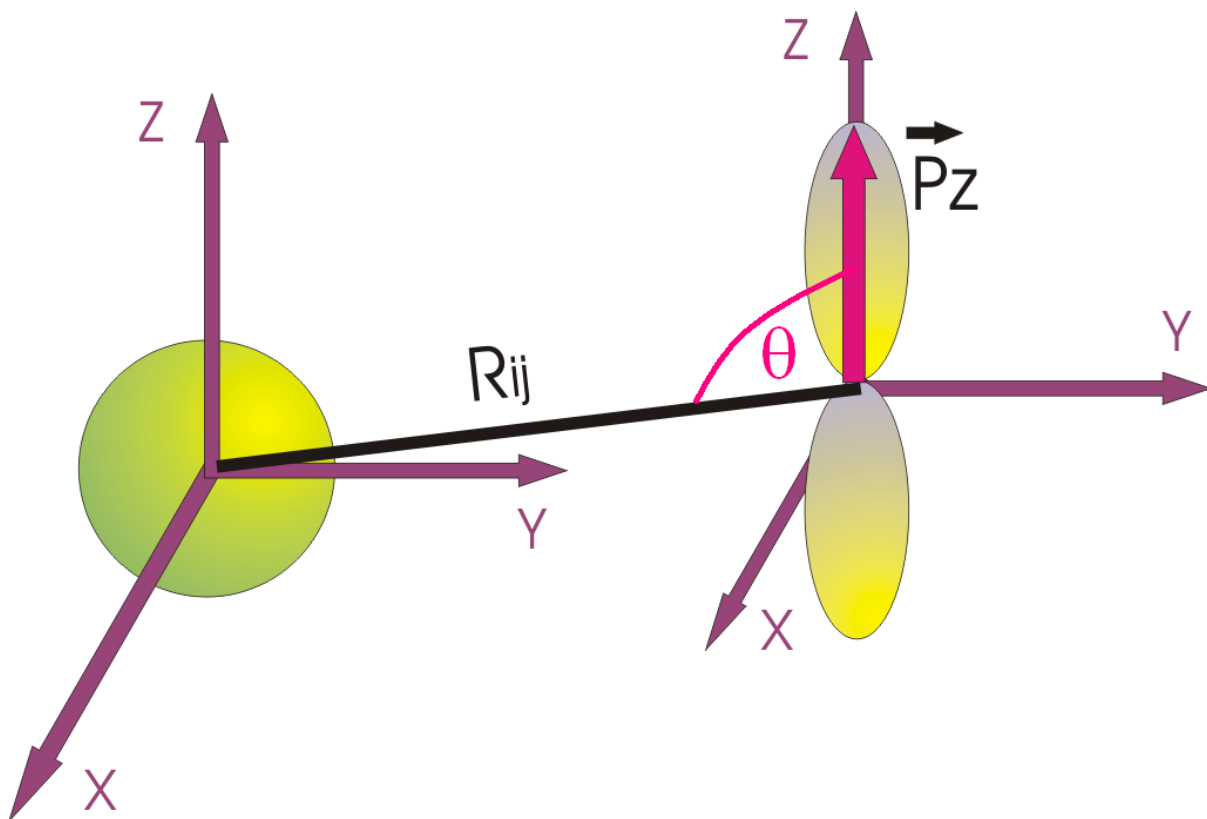
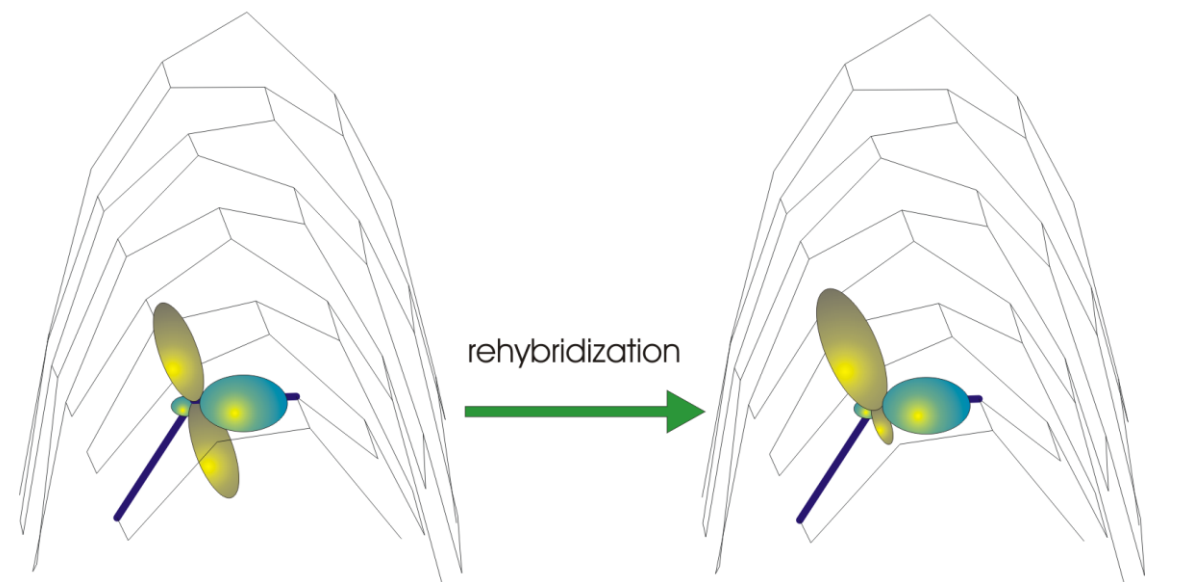


Fig.8. Schematic representation of the interaction of P_z - and S - orbitals.

As well known, the expression for the energy of the interaction between S and P -orbitals can be defined very simple:

$$V_{SPz}(r_{ij}) = V_{SPz}^{\sigma}(r_{ij}) \cdot \cos \theta \quad (18)$$



Presented scheme to reproduce the electronic configuration and the local bonding geometry around each atom provides the consideration and calculation of the rehybridization between σ - and π -orbitals. In Figure 9 we can see that the atom is in sp^2 hybridization becomes that in $sp^{2+\Delta}$ hybridization because of a curvature of the topological network.

Degree of rehybridization is defined on the pyramidalization angle. This angle is calculated on formula:

$$\theta_p = \theta_{\sigma\pi} - \frac{\pi}{2}.$$

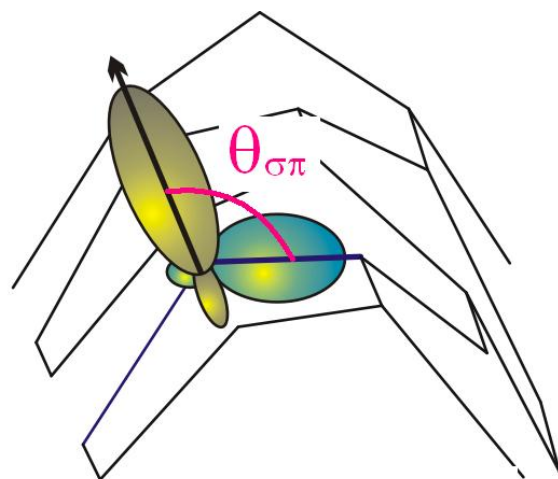


Fig.9. Rehybridization

Angle $\theta_{\sigma\pi}$ is presented as shown in Figure 9. π -orbital axis vector makes equal angles to the σ -bonds at a conjugated carbon atom.

To research the nanoribbons using tight-binding potential our own program was used. Own program provides the calculation of the total energy of nanostructures, which consist 500-5000 atoms. We have adapted our TB method to be able to run the algorithm on a parallel computing machine (computer cluster).

During consideration of the algorithm we can note two points:
 solution of eigenvalues problem and, possibly, eigenvectors problem for the $M \times N \times M \times N$ matrix - one-electron Hamiltonian (N is the the number of atoms, M is maximum number of valence electrons);
 - solution of optimization problem – the total system energy minimization.

It's necessary to consider the available computing power.

We have a number of dual-processor servers which are the distributed SMP-system. MPI (stands for Message Passing Interface) was choosen as mechanism for implementing parallelism.

Some note about optimization.

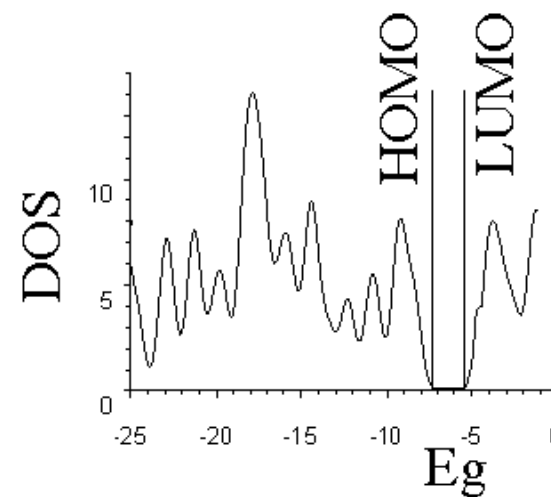
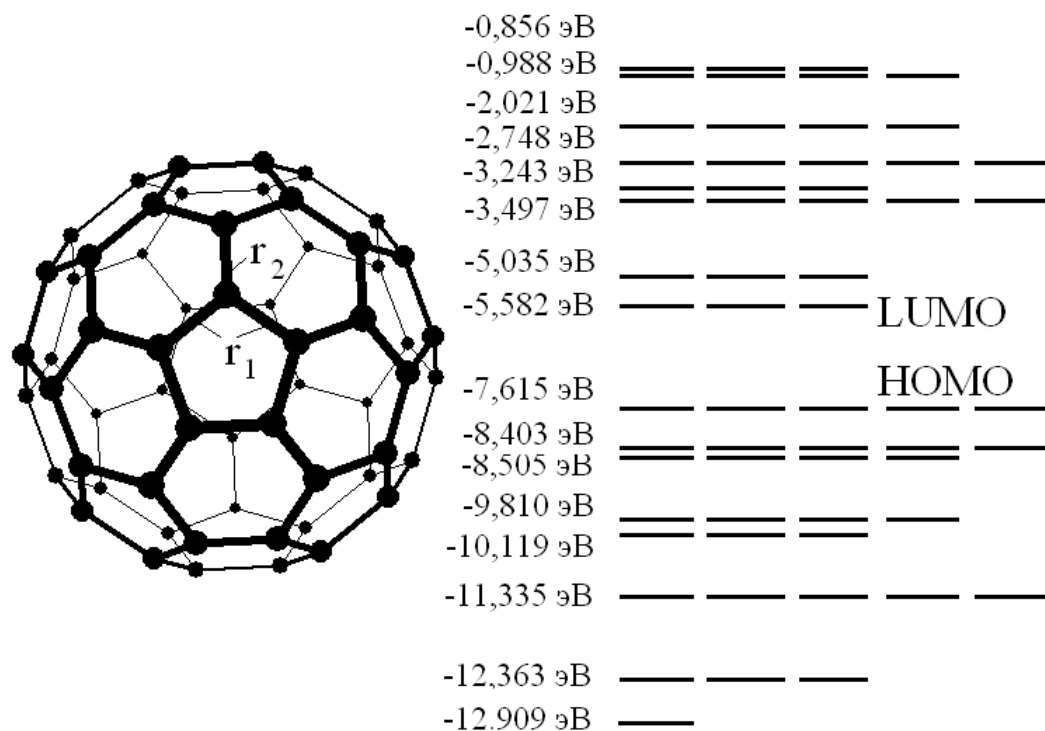
When choosing a method of **optimization**, we took into account the fact that we can't make any assumption about the nature and behaviour of target function. The target function in this case is the function of the total system energy of atoms coordinates. Also the analytics form of this function is unknown. That's why we have chose direct search optimization methods, in particular the Hook-Jeeves method. This method is one of the fastest modifications of coordinate descent methods and provides rapid convergence. We have decided to refuse the global search techniques at this stage because of its excessive computational complexity, which is the result of multiple calculations of target function. Also we assumed that theoretically found initial approximation is located in a small neighbourhood of global optimum.

First, we run our program that computes the target function values in different points from range of definition, with number of MPI threads equal to the number of available cores. But it was observed that in this case significant performance decrease occurs in calculation compared with the same single computation in one thread. This fact can be explained by the large amount of memory used for calculation, insufficient L2 cache and bottleneck in bandwidth of memory bus. To work around this we decided to use the hybrid OpenMP+MPI model in which data transfer between cluster nodes (parallel optimization process) is done with MPI and calculation within the node (target function calculation) is done with OpenMP. Experimentally we have found most effective ratio in terms of computing speed and the use of available resources for the problem: target function is calculated in 4 threads on one processor using OpenMP, data transfers between processors are implemented using MPI.

So, the presented transferable tight-binding potential and the described scheme to reproduce the electronic configuration and the local bonding geometry around each atom are well suited for computer simulations of covalently bonded systems in both gas-phase and condensed-phase systems.

We have tested our scheme by comparison with experiments for fullerene and some carbon nanotubes. In the table the spectra of the π -orbitals and density of states are presented.

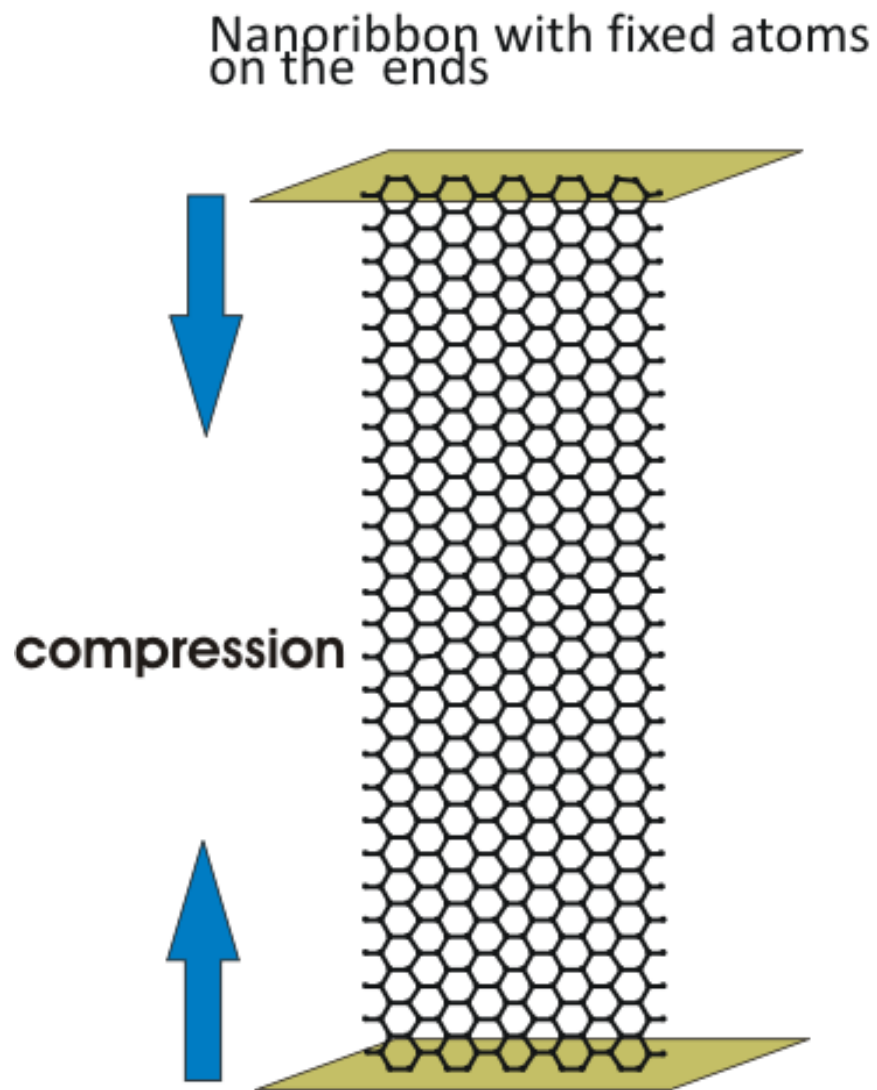
Results are in reasonable agreement with experimental data.



$$IP = 7.61 \text{ eV}, E_g = 2 \text{ eV}$$

$$r_1 = 1.45 \text{ \AA}, r_2 = 1.40 \text{ \AA}.$$

Fig.10. Fullerene C_{60} and the spectra of π -orbitals



*Armchair-nanoribbon undergoing axial
compression*

Atoms on the ends were fixed on the plates. The plates were moved towards each other to decrease the length for some percent.

Fig.11.

Compression of an armchair-nanoribbon with the ratio $L/D=3.22$:

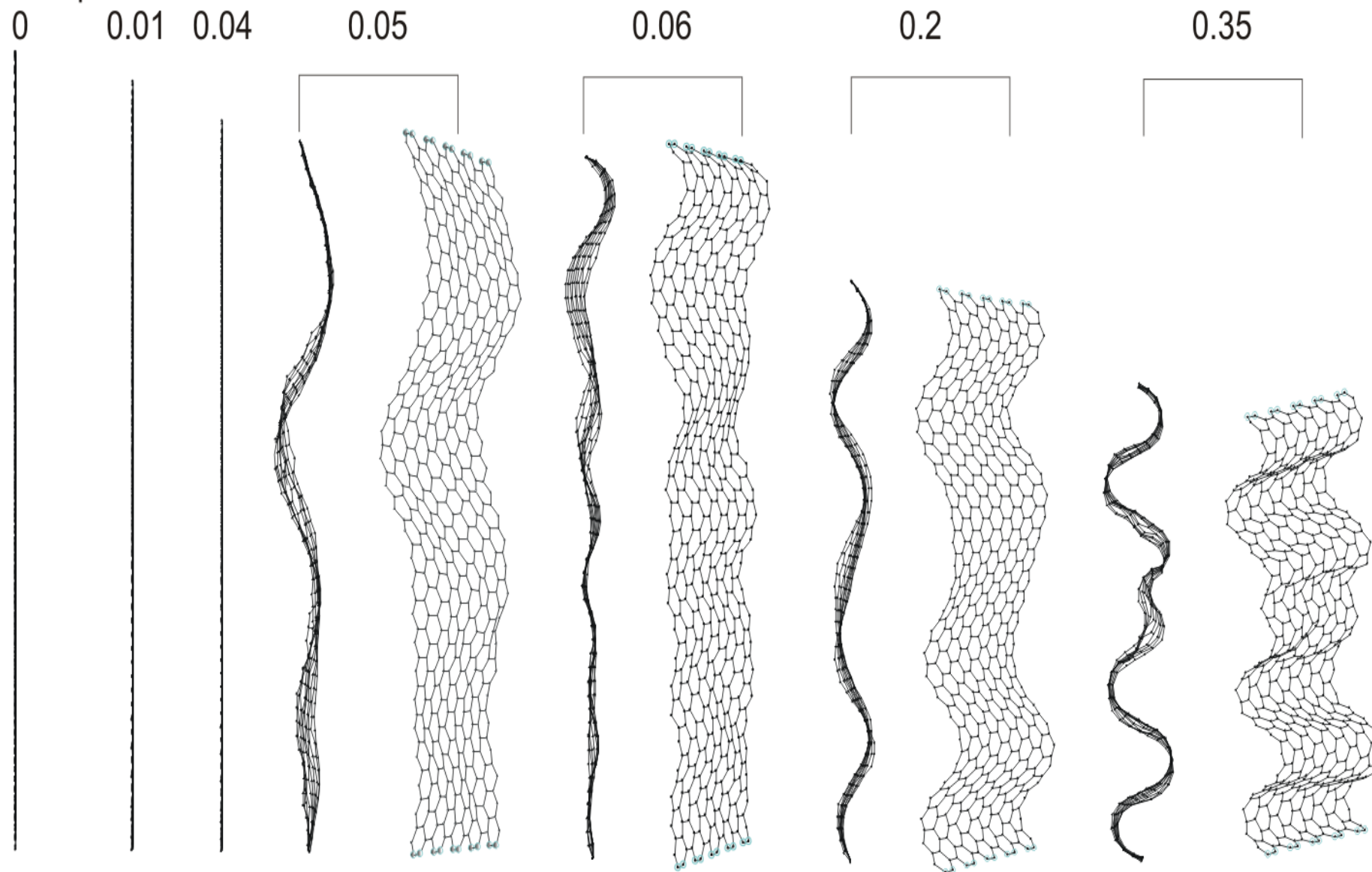


Fig.12

Plane network undergoing axial compression becomes wave-like. This is, so called, a phase transition.

Calculation of density of states demonstrates absence of changes in electronic structure.

However, the topology has nonzero pyramidalization angles.

Amplitude of a wave and its period are not constant and change along axis.

pyramidalization angles

$$\theta_p = \theta_{\sigma\pi} - \frac{\pi}{2}$$

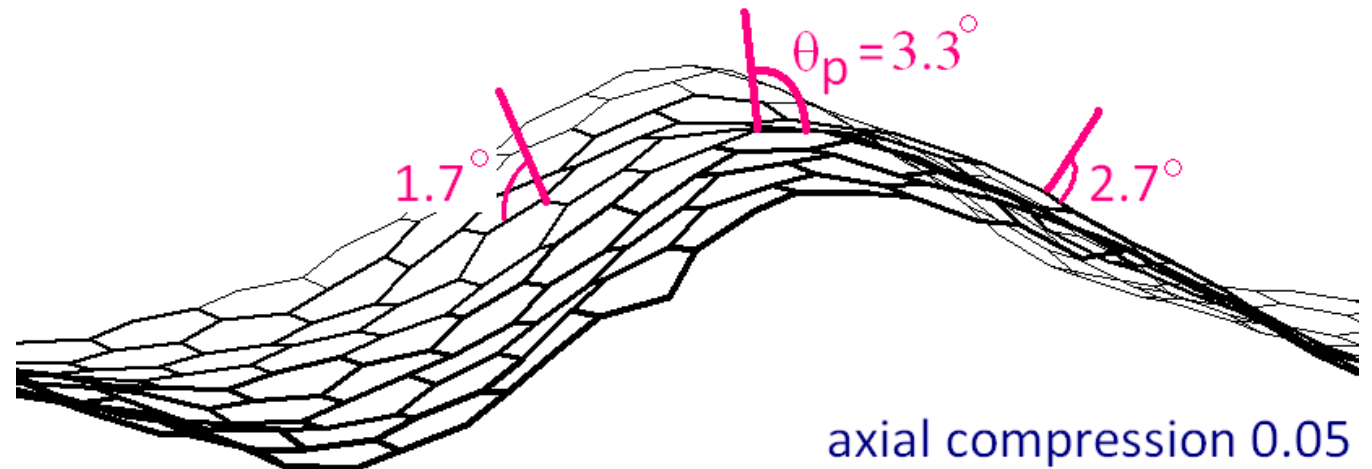


Fig.13.

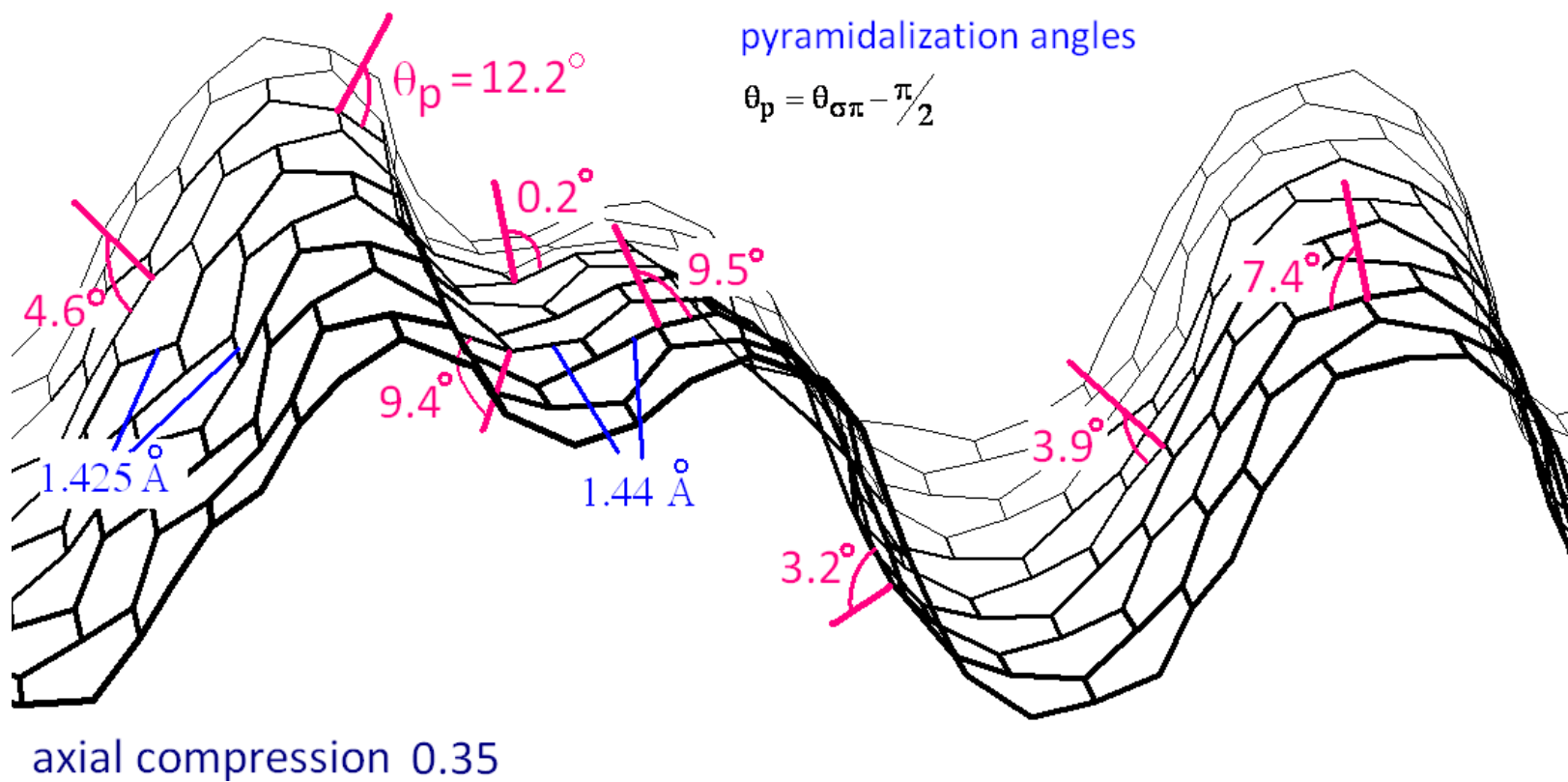


Fig.14.

Curvature of the atomic network because of compression will decrease the reactivity of the nanoribbon.

Compression of a zigzag-nanoribbon with the ratio $L/D=3.21$:

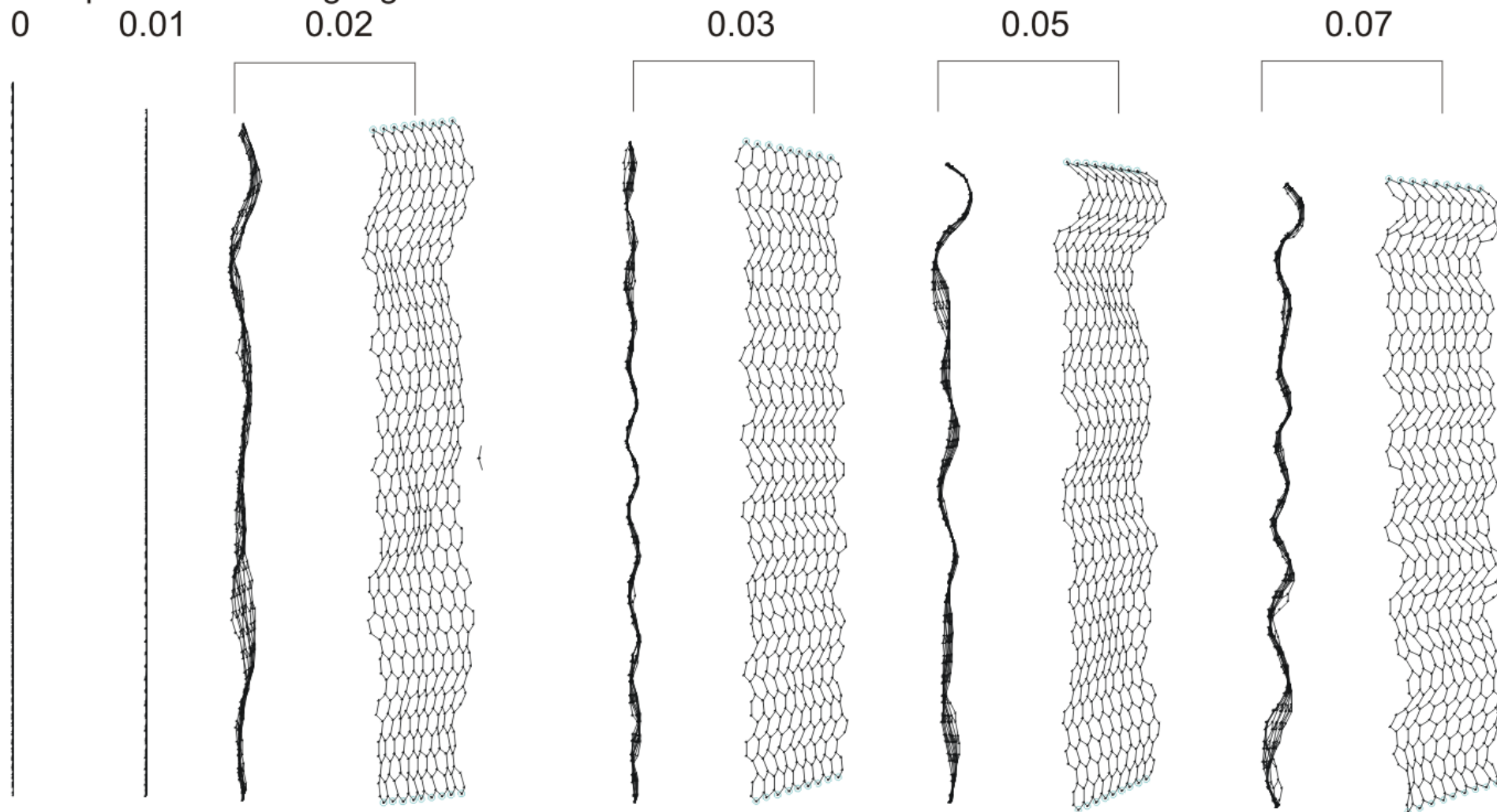


Fig. 15. Zigzag-nanoribbons undergoing axial compression

pyramidalization angles

$$\theta_p = \theta_{\sigma\pi} - \frac{\pi}{2}$$

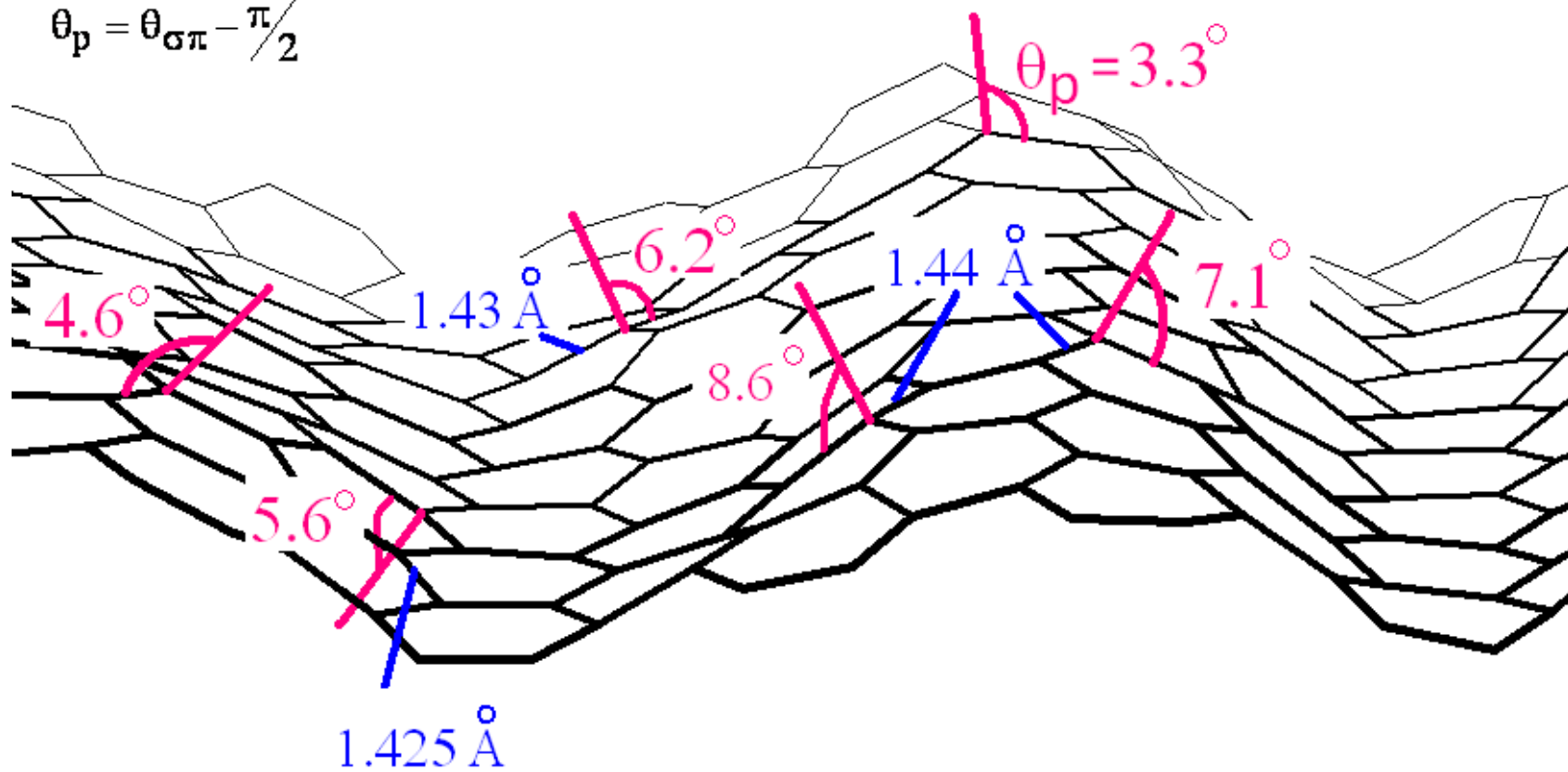


Fig. 16

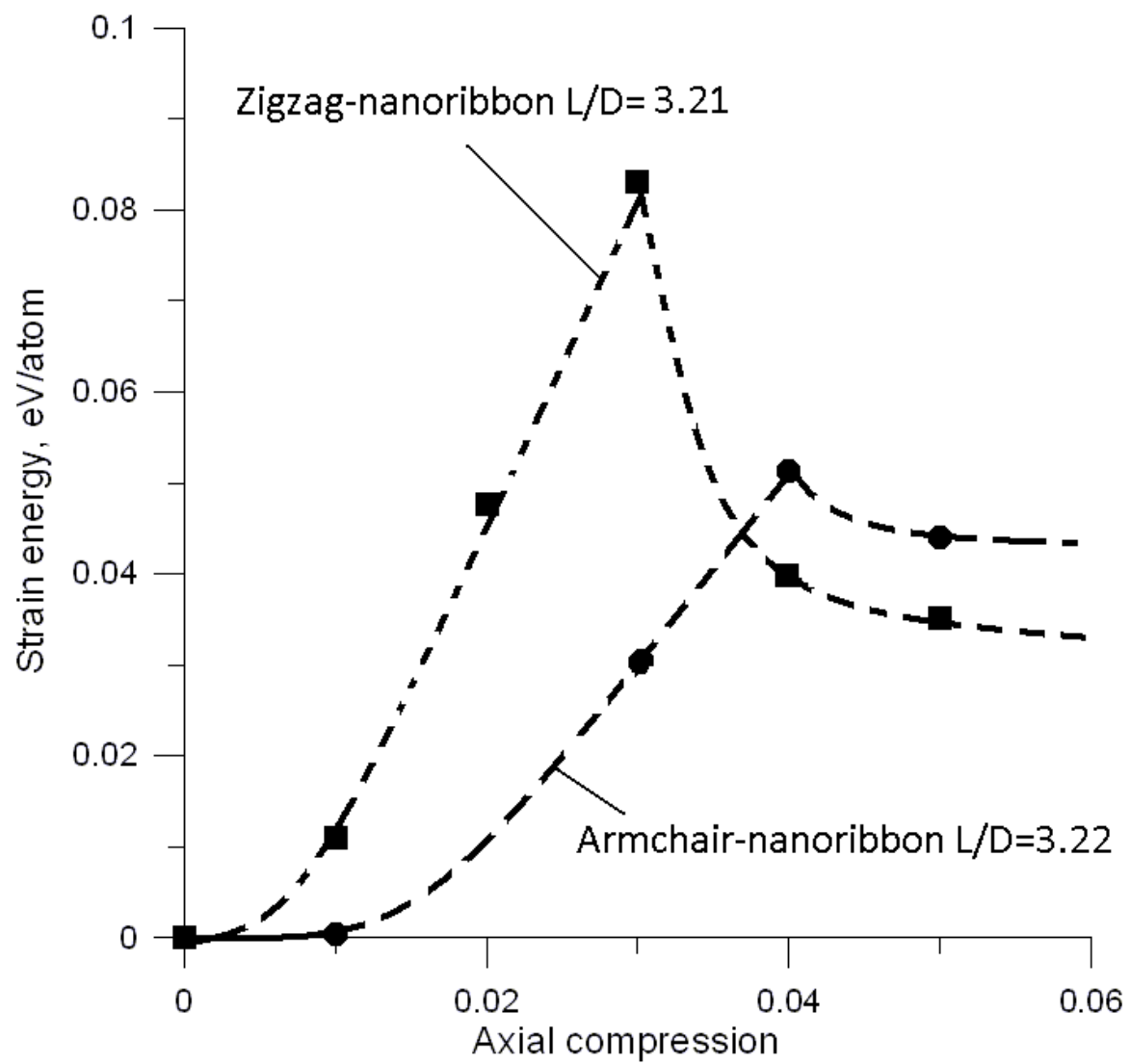
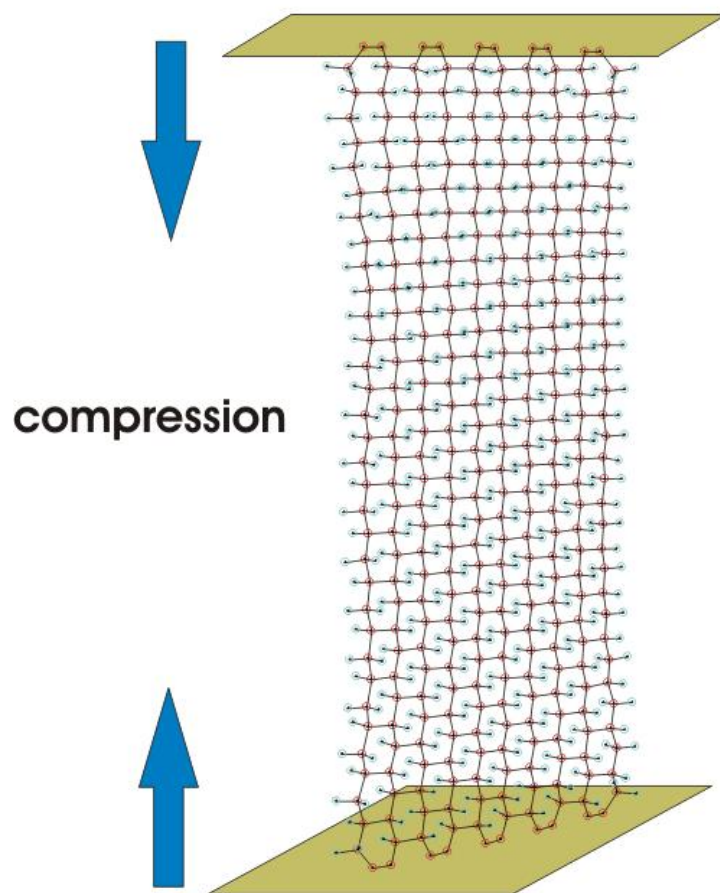


Fig. 17

Tight-binding calculation of the strain energy of nanoribbons undergoing axial compression.

Graphane-nanoribbons: chair-conformation

**Graphane -nanoribbon with
fixed carbon atoms on the ends**



*Armchair-nanoribbon undergoing axial
compression*

Carbon atoms on the ends were fixed on the plates. These atoms had no bonding with hydrogen atoms.

The plates were moved on a meeting each other to decrease the length for some percent.

Fig. 18

Compression of a armchair-graphane-nanoribbon with the ration $L/D=2.06$:

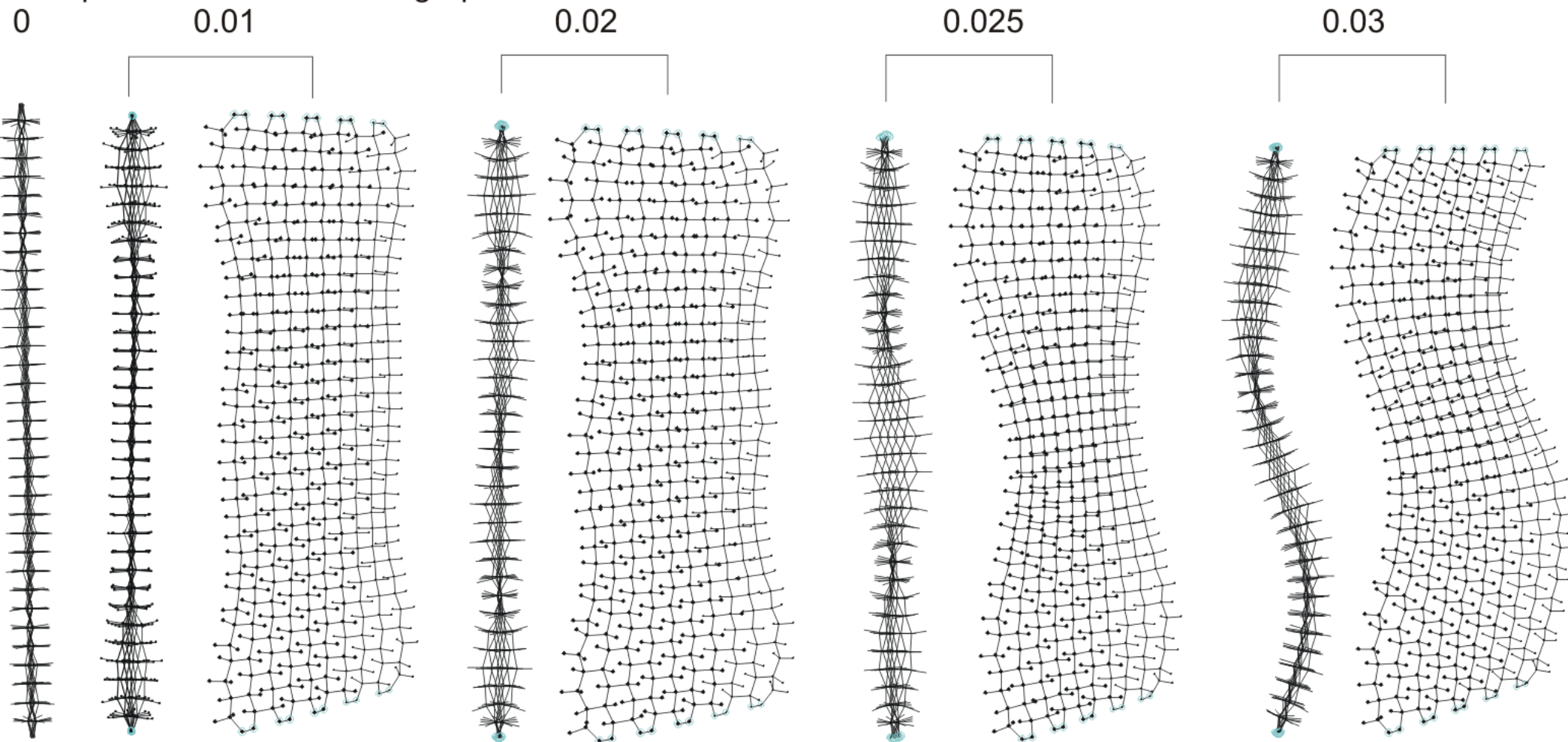


Fig. 19

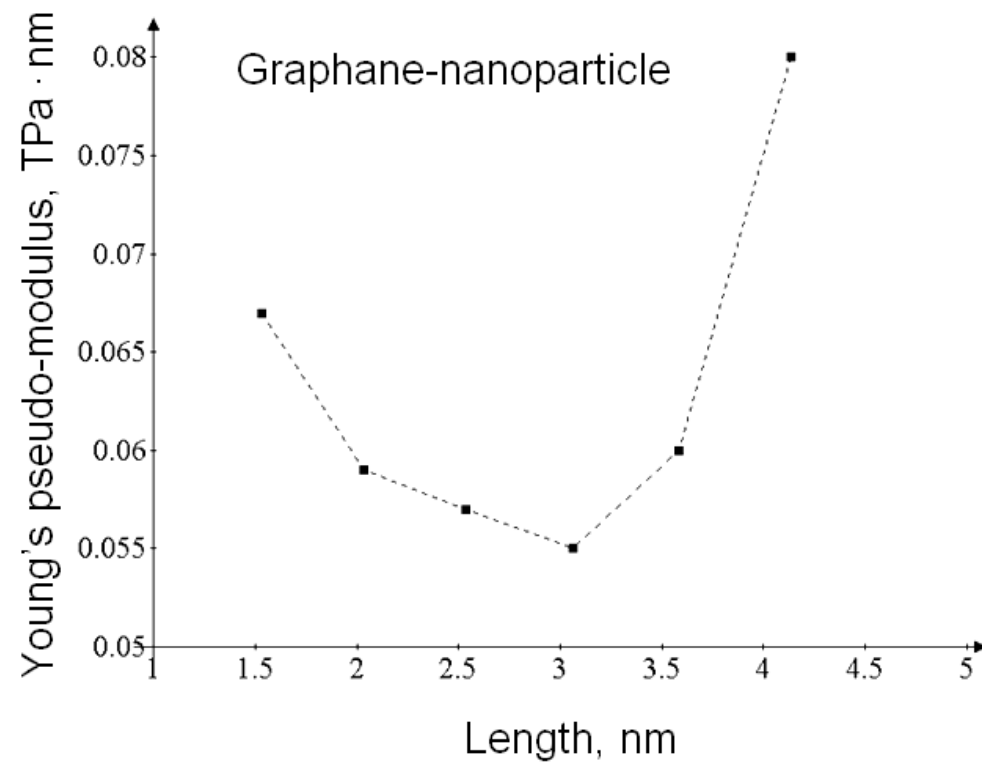
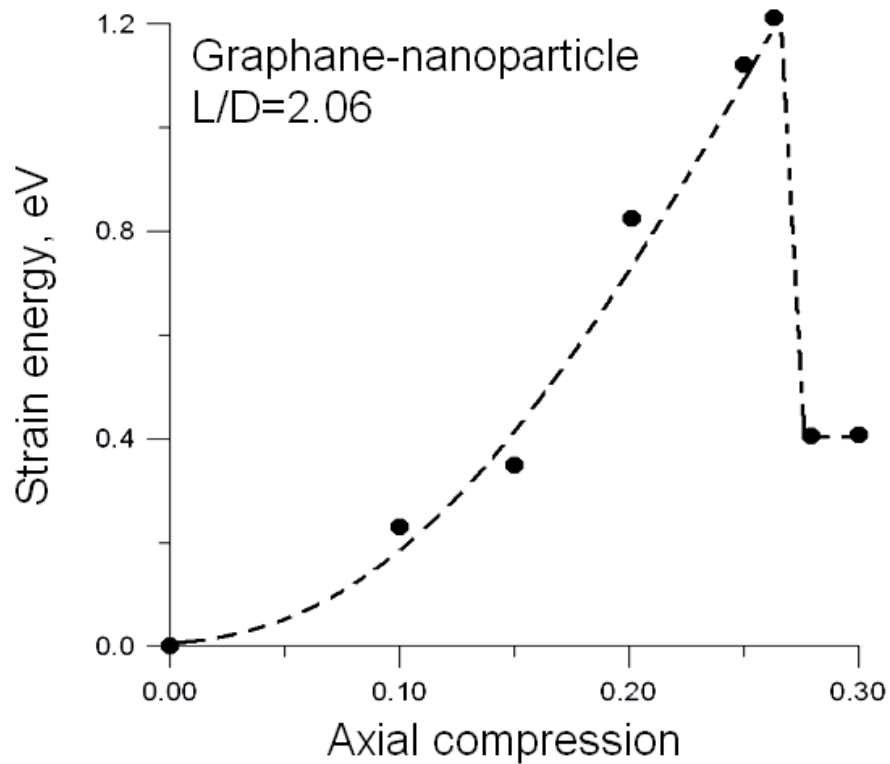


Fig. 20. Strain energy of nanoribbons undergoing axial tension

Fig. 21. Young's modulus of nanoparticle undergoing axial tension